Letter | Editors' Suggestion

Sound Waveguiding by Spinning: An Avenue toward Unidirectional Acoustic Spinning Fibers

Mohamed Farhat,[1] Pai-Yen Chen,[2] and Ying Wu[1,3,*]

[1] *Computer, Electrical, and Mathematical Sciences and Engineering Division, King Abdullah University of Science and Technology (KAUST), Thuwal 23955-6900, Saudi Arabia*

[2] *Department of Electrical and Computer Engineering, University of Illinois at Chicago, Chicago, Illinois 60607, USA*

[3] *Physical Science and Engineering Division, King Abdullah University of Science and Technology (KAUST), Thuwal 23955-6900, Saudi Arabia*

(Received 10 November 2022; revised 22 March 2023; accepted 23 March 2023; published 26 April 2023)

Waveguiding in general and acoustic waveguiding in particular are possible under the condition of a transverse "discontinuity" or modulation in the refractive index. We propose a radically different approach that relies on imposing spinning on a column of air, leading to highly modified acoustic refractive indices for specific azimuthal modes. This result may be leveraged to realize not only the airborne acoustic counterpart of an optical fiber, i.e., an acoustic spinning fiber, but also a nonreciprocal unidirectional waveguiding mechanism, reminiscent of an "acoustic Zeeman effect." The concept is demonstrated in the realm of acoustics, but may be applicable to other wave systems, e.g., in elastodynamics.

DOI: 10.1103/PhysRevApplied.19.L041002

Metasurfaces and metamaterials, consisting of periodically distributed unit-cells (or meta-atoms) in two and three dimensions, respectively [1], have revolutionized the way in which optical wave propagation can be controlled, leading to a broad range of applications from superlensing [2], invisibility cloaks [3], and optical waveguides [4] to computing [5]. Such concepts have been extended to other fields, including, but not limited to, acoustic [6–9], elastic [10,11], structural [12], and thermodynamic [13] waves. In particular, acoustic waveguiding for airborne sound requires a relative acoustic refractive index greater than one or, equivalently, a speed of sound lower than that in air (343 m/s at room temperature) [14], which is almost impossible for normal materials. Metamaterial structures may result in an effective refractive index with the required behavior, such as in the case reported in Ref. [15], which needs subwavelength structuring, but the effect is limited to narrow-band operation. Recently, in optics, a different strategy has been suggested that exploits the vectorial spin-orbit interaction of light and its geometric phases [16]. However, this approach is infeasible in acoustics, as it requires anisotropic media with tailored optical axes. Instead, acoustic spin transport in waveguides [17] and spin redirection for topological sound transport [18–20] have been suggested. The realization of a high-refractive-index material for airborne sound waveguiding remains a major challenge.

Recently, time-varying metamaterials have been proposed as a promising paradigm [21,22] for designing intriguing functionalities such as those of luminal devices [23] and amplifying structures [24,25]. In the same vein, the use of acoustic metamaterials with moving components to enrich the application spectrum has been put forward [26–32]. For instance, spinning acoustic fluids have been shown to possess scattering-cancellation properties [33] and to lead to a negative acoustic torque and force without a transverse variation of the refractive index [34]. These metamaterials with spinning components have also been shown to break reciprocity [35,36] and to lead to topological acoustics [37]. More recently, spinning metasurfaces have been employed to nonreciprocally generate acoustic vortex beams [38] and to passively convert sound frequencies [39]. However, in these studies the medium was at rest and only the metasurface was rotating, and so the spinning motion did not generate waveguiding. These achievements naturally inspired us to consider the spinning of air columns as a candidate for realizing the confinement and waveguiding of sound, which in this case obeys a modified (azimuthally dependent) Helmholtz-like equation with a modified wave number for an effective anisotropic medium [33].

*ying.wu@kaust.edu.sa

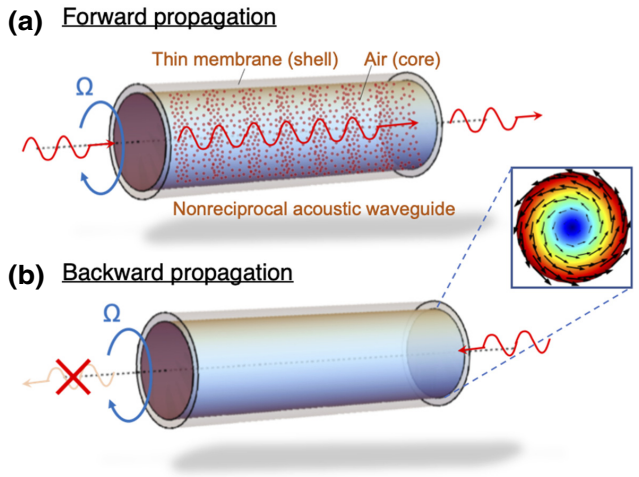

FIG. 1. Schematic illustration of an ASF spinning at an angular frequency Ω (in rad/s): (a) forward (allowed) propagation; (b) backward (forbidden) propagation. A thin membrane separating spinning air and air at rest is shown schematically; the dots show schematically the air particles under the influence of the background acoustic field. The black arrows in the inset show the profile of the background-flow velocity field computed with COMSOL [40] [red (blue) color corresponds to high (low) velocity].

In this Letter, we propose an alternative mechanism for acoustic waveguiding, namely the use of an acoustic spinning fiber (ASF), which leverages the effect of the spinning fluid inside the ASF (see Fig. 1). Spinning induces an anisotropic effective acoustic refractive index, whose component in the longitudinal (z) direction is greater than 1 ($n^z_{\text{eff}} > 1$) for some multipolar modes, representing an important step beyond naturally occurring materials. This satisfies the condition for confinement and waveguiding along with the transverse wave number being real-valued (see the Supplemental Material [41] for a detailed derivation). We consider an acoustic fiber with the same physical properties as the surrounding air (an impedance-matched thin membrane may isolate the fiber from the exterior: this can be realized, for example, via a sound-permeable thin-sheet solid material [42]). We then show in particular that the multipoles $m = +1$ and $m = +2$ can be used for confinement and waveguiding, thus realizing the equivalent of an optical fiber. Analytical and numerical [41] models (based on the linearized Navier-Stokes interface of COMSOL Multiphysics [40]) and Hamiltonian modeling demonstrate the robustness of this concept with respect to leaking and may form a basis for several exciting functionalities requiring airborne acoustic waveguiding. We show further the spinning-induced unidirectionality of this guiding process, with promising applications such as in airborne sound-based communication.

Problem setup.—Acoustic pressure waves in a spinning nonviscous fluid (air in this study), as shown schematically in Fig. 1, obey a Helmholtz-like wave equation (see the Supplemental Material [41] for a detailed derivation) with an equivalent spinning (azimuthally dependent, i.e., dependent on m) wave number $k_m^2 = \kappa^2 + \eta_m^2 k^2 = -\left(4\Omega^2 + \gamma_m^2\right)/c^2$, where c is the speed of sound, p is the pressure field, and the anisotropy parameter is $\eta^2 = 1 + 4\Omega^2/\gamma_m^2$. Ω denotes the spinning angular frequency, and $\gamma_m = -i(\omega - m\Omega)$ is the azimuthal Doppler angular frequency, with $m \in \mathbb{Z}$. When $\Omega \to 0$, we recover $k_m = \omega/c$ and $\eta_m = 1$, $\forall m$. The features of the spinning wave numbers k_m are characterized in Ref. [33] and further in the Supplemental Material [41]. Since γ_m is a complex-valued parameter, k_m has both propagating (real part) and evanescent (imaginary part) components. There are also frequencies $\omega = (m \pm 2)\Omega$ where $k_m \approx 0$, reminiscent of the behavior of near-zero-index metamaterials. As an illustration, a few multipole mode dispersions in terms of the effective refractive index [$n^t_{\text{eff}} = k_m/k_0$ and $n^z_{\text{eff}} = k_m/(k_0\eta_m)$] are plotted as functions of frequency in Fig. 2. Here, the angular frequency Ω is equal to 100 rad/s (clockwise). It is observed that, for low frequencies, the imaginary part of n^t_{eff} dominates, while the real part is zero. For a given mode order m, the imaginary part vanishes at a specific frequency, while the real part increases and converges toward a specific value. In the low-frequency regime, there is thus no propagation, due to finite imaginary part of n^t_{eff}. This evanescent regime is highlighted by the gray regions in Fig. 2. Regarding the propagation regime, we are thus interested in modes with $(n^t_{\text{eff}})^2 > 0$ and $n^z_{\text{eff}} > 1$. For $m = 0$ or $m = -1$, this condition is obviously not satisfied. However, for $m = 1$ and $m = 2$, a markedly different behavior is noted. For instance, for $m = 1$, starting from a finite angular frequency ($\Omega = -100$ rad/s, i.e., a spinning frequency $|\Omega|/2\pi \approx 16$ Hz), we have $n^z_{\text{eff}} > 1$. For $m = 2$, waveguiding occurs even at zero frequency [41]. Hence, for $m = 1, 2$, confinement of sound waves and waveguiding are both possible.

Consider a circular air waveguide wrapped by a thin impedance-matched membrane (which serves as an artificial separation of the spinning fluid and the fluid at rest, while being transparent to sound [43]), as shown schematically in Fig. 1. At the interface between the spinning waveguide and the host medium, proper continuity conditions need to be satisfied. Namely, the pressure field p and the normal displacement ζ_r^m (see the Supplemental Material [41] for expressions) are continuous. Suppose the radius of the waveguide is r_1; the spinning air inside it is denoted by the subscript 1, and the surrounding air at rest is denoted by the subscript 2. We assume that these media are nonviscous and ignore effects due to friction, as the system is airborne (see Section I of the Supplemental Material [41] for more details). This kind of system models a step-index ASF.

As shown schematically in Fig. 1, in each medium ($r < r_1$ and $r \geq r_1$) the pressure field obeys the Helmholtz

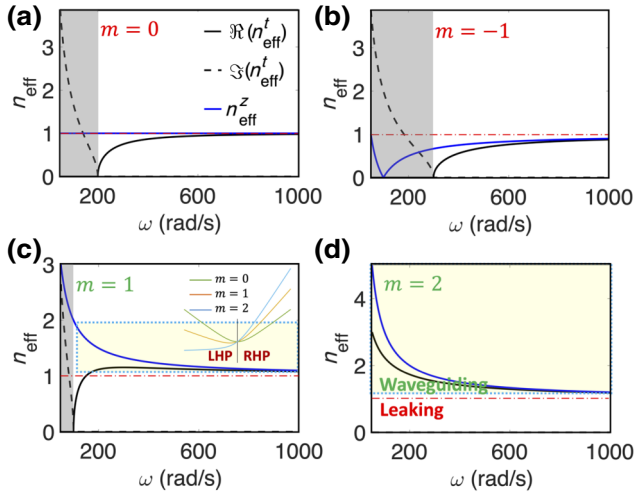

FIG. 2. Spinning column of fluid with angular frequency $\Omega = -100$ rad/s. A negative (positive) sign for the spinning angular frequency means that the spinning is clockwise (anticlockwise). Dispersion relations are shown in this case for (a) $m = 0$, (b) $m = -1$, (c) $m = 1$, and (d) $m = 2$. The continuous (dashed) lines give the real (imaginary) parts of n^t_{eff}, while the blue lines plot n^z_{eff}. The upper (lower) regions with respect to the red dotted-dashed lines correspond to waveguiding (leaking or radiation). The yellow (gray) transparent boxes show the waveguiding (evanescent) regime. The inset in (c) gives the frequency as a function of Ω/k_0 for symmetrical ($m = 0$) and asymmetrical ($m = 1, 2$) left-hand propagation (LHP) and right-hand propagation (RHP).

equation, but with different transverse wave numbers κ_1 and κ_2. The pressure fields have to be finite at $r \to 0$, indicating that $p_1 = a_m J_m(\kappa_1 r) e^{im\phi} e^{ikz}$ for $r < r_1$, and satisfy the Sommerfield radiation condition, meaning that $p_2 = b_m H^{(1)}_m(\kappa_2 r) e^{im\phi} e^{ikz}$ for $r \geq r_1$, for the mode of order m. The unknown coefficients a_m and b_m can be derived by considering the boundary conditions. In passive media (no loss or gain, which is assumed in this study), κ_1^2 and κ_2^2 are purely real numbers. To confine propagation inside the waveguide (or ASF, i.e., for $r < r_1$), we have to enforce $\kappa_1 = \kappa > 0$ and let $\kappa_2 = i\beta$ (where β is a positive real number) such that the pressure field decays far from the ASF. κ and β satisfy the dispersion relations [41]

$$\kappa^2 = \frac{\omega^2}{c_1^2}\left[(m\alpha - 1)^2 - 4\alpha^2\right] - \eta_m^2 k^2, \quad \beta^2 = k^2 - \frac{\omega^2}{c_2^2}, \tag{1}$$

where c_1 and c_2 are the acoustic wave speeds in the ASF and in the surrounding air, respectively, $\alpha = \Omega/\omega$ is the dimensionless spinning ratio, and k is the propagation constant of the waveguided mode inside the ASF. The peculiar dispersion inside the spinning medium arises from the unique governing equation. The fields can thus be rewritten using modified Hankel functions, i.e., $p = a_m J_m(\kappa r) e^{im\phi}\, e^{ikz}$ for $r < r_1$ but $p = b_m K_m(\beta r) e^{im\phi}\, e^{ikz}$ for

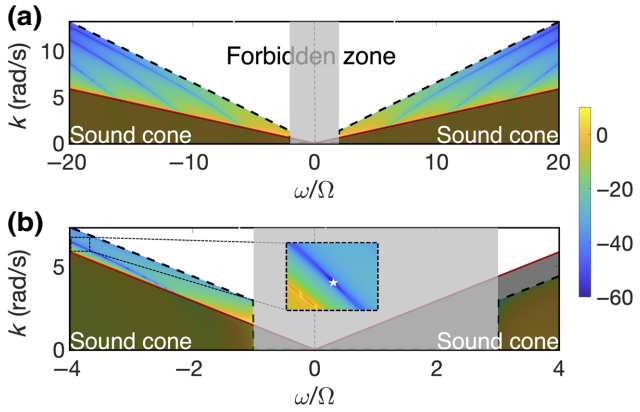

FIG. 3. Contour plot of the dispersion relation of (a) mode $m = 0$, i.e., $10 \times \log_{10}(|F_0(\omega, k)|)$, and (b) mode $m = 1$, i.e., $10 \times \log_{10}(|F_1(\omega, k)|)$, versus ω/Ω and k, represented by Eq. (3). The gray zone denotes the evanescent regime of k_m.

$r \geq r_1$ [where we choose to keep the notation b_m, even if there is a proportionality factor of $(\pi/2)i^{m+1}$]. This choice ensures that the acoustic wave does not propagate energy toward the exterior of the ASF (i.e., leaking), as the fields decay exponentially with r ($\lim_{r\to+\infty} |p| = 0$).

Spinning-induced acoustic fiber.—The $m = 0$ mode does not result in $n^z_{\text{eff}} > 1$ and therefore is not a waveguided mode, as shown in Fig. 2(a). Yet it is interesting to briefly analyze this fundamental mode to understand the basic effects. We suppose that a column of a fluid with $n_1 = \sqrt{5}$ and radius r_1 is spinning, and we apply convenient boundary conditions at $r = r_1$. Although for this fundamental mode waveguiding is not induced by spinning but rather by $n_1 > 1$ inside the fiber, the spinning still has some intriguing effect on the dispersion [as seen in Fig. 3(a)] and the induced waveguiding overall (see Section III and Fig. 1 in the Supplemental Material [41] for a detailed discussion of the fundamental-mode-based waveguiding mechanism).

For higher-order modes, we investigate acoustic waveguiding induced solely by spinning, which thus does not require a refractive index greater than 1. We consider a medium with the same properties as the surrounding air and analyze the waveguiding effect. Hence, it is obvious that the waveguiding mechanism differs drastically from those previously investigated (including optical waveguiding). Here, the confinement of the acoustic fields inside the ASF is induced not by an increased refractive index, but rather by the spinning dynamics only. This is manifested by Eq. (1), which can lead to

$$\frac{\kappa^2}{\eta_m^2} + \beta^2 = \frac{\omega^2}{c^2 \eta_m^2}\left[(m\alpha - 1)^2 - 4\alpha^2 - 1\right] \tag{2}$$

if $c_1 = c_2 = c_{\text{air}} = c$.

To allow guided modes, both κ and β should be real numbers (so as to ensure propagation in the core for

$\kappa_1 = \kappa$ and exponential decay in the surroundings via $\kappa_2 = i\beta$), which requires that the rhs of Eq. (2) is positive. When we allow different material properties ($n_1 > n_2$, i.e., $c_1 < c_2$) without spinning, this condition is just $1/c_1^2 - 1/c_2^2 > 0$. But in Eq. (2) this condition becomes $(m\alpha - 1)^2 - 4\alpha^2 \geq 1$ in the propagation regime, or, equivalently, $\alpha\left[\left(m^2-4\right)\alpha - 2m\right] \geq 0$. This inequality explains the findings in Fig. 2, where waveguiding is possible only for $m = 1$ or $m = 2$ for $\Omega = -100$ rad/s (see Fig. 3 in the Supplemental Material [41] for details). Now, by applying the more general boundary condition for the multipole m, we can get the dispersion equation

$$\begin{vmatrix} J_m(\kappa r_1) & -K_m(\beta r_1) \\ \dfrac{\left(2\Omega^2 - \gamma_m^2\right)\kappa J_m'(\kappa r_1) - (3\gamma_m \Omega i m/r_1) J_m(\kappa r_1)}{\rho_1\left(4\Omega^2 + \gamma_m^2\right)\left(\Omega^2 + \gamma_m^2\right)} & -\dfrac{1}{\rho_2\omega^2}\beta K_m'(\beta r_1) \end{vmatrix} = 0, \tag{3}$$

with both κ and β satisfying Eq. (2); we denote the lhs of Eq. (3) by $F_m(\omega, k)$.

The dispersion resulting from this model is depicted in Fig. 3(b) for the case $m = 1$ (see Fig. 2(c) for the dispersion of the medium) and exhibits unique behaviors that are not observed in common waveguiding systems. The red solid line indicates the sound cone in the medium at rest, i.e., ω/c. The modes appearing below this line correspond to leaking modes (radiative regime), i.e., acoustic waves that propagate into the surrounding space. The black dashed line corresponds to a forbidden zone [neither propagating nor leaking modes are possible above the black dashed curve, i.e., the white region of the two-dimensional (2D) plot]. This curve does not start from zero, but rather has "cutoff" frequencies originating from the imaginary part of n_{eff}^t [i.e., solutions of $(\alpha - 1)^2 - 4\alpha^2 = 0$ [41]], as highlighted by the gray zones in Figs. 2 and 3. This frequency depends on the mode, indicating tunability of the acoustic waveguiding. Hence, it is confirmed that a column of air that is simply spinning results in confinement and waveguiding [the dark blue region of the 2D plot; see the inset of Fig. 3(b)]. Moreover, it is worth noting that this confinement is asymmetric, i.e., it results in a one-way waveguiding effect. For instance, Fig. 3(b) shows different dispersions for opposite spinning directions. This shows that sound waves propagating toward the right and the left are markedly distinct. For some frequencies, highlighted in Fig. 3(b), it is possible to enforce unidirectional propagation, where RHP is possible, while LHP is prohibited. Such a feature is not possible with classical waveguides and is reminiscent of spin-induced waveguiding [16] and vortex beams [44].

Mechanism of the ASF.—To get further insight into the intriguing findings discussed above (such as the nonreciprocal property), we define state vectors $|\psi\rangle = (p, \mathbf{v})^T$, where $(\cdot)^T$ is the transpose operator and $\mathbf{v} = (v_r, v_\phi, v_z)^T$, endowed with the scalar product $\langle\psi_1, \psi_2\rangle = \int_{\mathcal{V}} dV\left\{p_1^* p_2 + \mathbf{v}_1^* \cdot \mathbf{v}_2\right\}$, where $\mathcal{V}$ is the volume of the ASF. In this way, the governing equation [Eq. (5) in the Supplemental Material [41]] can be written in the more elegant way $\left[H^{(0)} + \delta H\right]|\Psi\rangle = \omega\,|\Psi\rangle$, where ω is the eigenfrequency of the system. $H^{(0)}$ (δH) is the time-evolution operator of the system in the absence of a bias (perturbation operator) (see the Supplemental Material [41] for expressions). It can be shown that in the absence of a bias ($\Omega = 0$), two modes exist ($m = \pm 1$) and have the same eigenfrequency ω, i.e.,

$$|\pm\rangle = \zeta_\pm \begin{pmatrix} i\rho\omega \\ \kappa_1 \dfrac{J_{\pm1}'(\kappa r)}{J_{\pm1}(\kappa r)} \\ \dfrac{\pm i}{r} \\ ik \end{pmatrix} \times J_{\pm1}(\kappa r)\, \frac{e^{i(kz \pm \phi)}}{i\omega\rho}, \tag{4}$$

where the constants $\zeta_\pm$ are renormalization factors [41], computed by using the scalar product defined above (see the Supplemental Material [41]).

When we turn spinning on (i.e., we have a biased system, with $\Omega \neq 0$), we make the assumption that the new eigenvectors lie in the subspace described by the unbiased waveguided modes given in Eq. (4) [35]. We can thus write the new eigenvectors as a linear combination of $|\pm\rangle$, with some unknown complex coefficients μ^+ and μ^-, i.e., $|\psi\rangle = \mu^+|+\rangle + \mu^-|-\rangle$. By using the fact that $H^{(0)}|\pm\rangle = \omega_0|\pm\rangle$, we obtain

$$\begin{pmatrix} \langle+|\,\delta H\,|+\rangle & \langle+|\,\delta H\,|-\rangle \\ \langle-|\,\delta H\,|+\rangle & \langle-|\,\delta H\,|-\rangle \end{pmatrix} \begin{pmatrix} \mu^+ \\ \mu^- \end{pmatrix} = (\omega - \omega_0) \begin{pmatrix} \mu^+ \\ \mu^- \end{pmatrix}, \tag{5}$$

where we have $\langle\pm|\,\delta H\,|\mp\rangle = 0$ and $\langle+|\,\delta H\,|+\rangle = -\langle-|\,\delta H\,|-\rangle$ [41]. Hence, the eigenvalues of the biased system are given by Eqs. (4) and (5) as

$$\omega^\pm = \omega_0 \pm \langle+|\,\delta H\,|+\rangle, \tag{6}$$

where $\langle+|\,\delta H\,|+\rangle = \Omega$ for the modes that we consider in this demonstration [41], i.e., $m = \pm 1$. This analysis

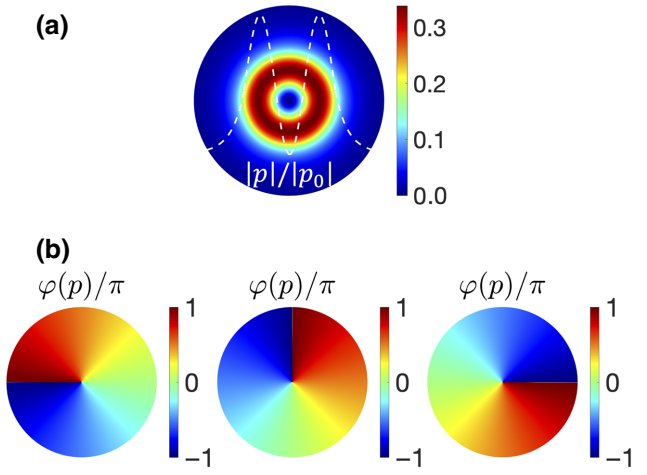

FIG. 4. (a) Snapshot of the normalized amplitude of the pressure field $|p|/|p_0|$ inside the ASF and outside it at the frequency highlighted by the white star in the inset of Fig. 3(b). The white dashed curve plotted on top of the amplitude is a section along the direction $\phi = 0$. (b) Snapshots of the phase [$\varphi(p)$ in units of π] of the pressure field p inside the ASF and outside it at three different locations in the propagation direction (z axis): from left to right, $z = 0$, $\pi/2k$, and π/k.

demonstrates that the spinning of the air breaks reciprocity, similarly to the application of a magnetic field in optics (the Zeeman effect) [45,46], and hence lifts the degeneracy of the eigenfrequencies corresponding to counterpropagating directions, as shown by Eq. (6). But this can occur only if $m \neq 0$, as for $m = 0$ the dispersion is symmetrical, which is verified in Fig. 3(a) and predicted by the dispersion shown in the inset of Fig. 2(c).

In the same vein, Fig. 4(a) depicts the pressure-field distribution, which not only shows the confinement, but also exhibits a minimum at the center of the ASF, indicating the presence of a singularity. A similar feature was observed previously for vortex beams carrying an acoustic orbital angular momentum (OAM) [44]. In our case, as was shown recently in Ref. [34], spinning fluids also carry a spin and orbital angular momentum. This may explain the singularity at the center of the ASF seen in Fig. 4(a). Moreover, Fig. 4(b) gives the phase of the pressure field (in units of π) at the point highlighted by the white star in Fig. 3(b) for different locations along the propagation axis (the z axis here), i.e., for $z = 0$, $\pi/2k$, and π/k, where k is the propagation constant taken from Fig. 3(b). This further confirms the orbital nature of this waveguiding phenomenon.

Discussion and conclusion.—In this Letter, we show spinning-induced acoustic waveguiding. We leverage the rotation of a spinning column of air (surrounded by air, too) to obtain intriguing azimuthally dependent dispersion with an anisotropic effective refractive index. For specific parameters, we analyze the condition for confinement of airborne sound and describe in detail the resulting acoustic spinning fiber. In particular, the suggested mechanism is endowed with several intriguing properties, such as (i) unidirectionality of propagation due to the asymmetry in the dispersion of the waveguide modes and the acoustic analog of the Zeeman effect, (ii) the presence of a singularity in the pressure field reminiscent of an acoustic OAM, and (iii) tunability of the waveguiding by tuning or flipping the sign of the spinning angular frequency. Moreover, the proposed ASF is the acoustic counterpart of an optical fiber, for which one of the main advantages is an enhanced bandwidth and low loss compared with hollow electric waveguides [47]. Thus, the proposed ASF may possess an enhanced bandwidth and offer longer propagation distances, as it does not suffer from absorption loss or undesired reflections (the reflection channel is forbidden by the nonreciprocal behavior). All of these properties demonstrate the potential of this ASF, which can be applied in several domains, including airborne sound communication (by avoiding undesired parasitic back reflection), and to shed light on the physics of acoustic vortex beams and nonreciprocal physics.

Although an experimental demonstration of this concept is outside the scope of the present Letter, some recent experimental studies indicate that our proposal may be demonstrated (see the Supplemental Material [41]) using similar configurations [35,36]. Moreover, the COMSOL-based [40] simulations shown in the Supplemental Material [41] further demonstrate the accuracy of our model.

Acknowledgments.—This work was supported by the King Abdullah University of Science and Technology (KAUST) Office of Sponsored Research (OSR) under Grant No. OSR-2020-CRG9-4374, as well as the KAUST Baseline Research Fund, Grant No. BAS/1/1626-01-01.

[1] W. Cai and V. M. Shalaev, *Optical Metamaterials* (Springer, New York, 2010), Vol. 10.
[2] N. Fang, Z. Liu, T.-J. Yen, and X. Zhang, Regenerating evanescent waves from a silver superlens, Opt. Express **11**, 682 (2003).
[3] H. Chen, C. T. Chan, and P. Sheng, Transformation optics and metamaterials, Nat. Mater. **9**, 387 (2010).
[4] M. Kadic, S. Guenneau, S. Enoch, P. A. Huidobro, L. Martin-Moreno, F. J. García-Vidal, J. Renger, and R. Quidant, Transformation plasmonics, Nanophotonics **1**, 51 (2012).
[5] A. Silva, F. Monticone, G. Castaldi, V. Galdi, A. Alù, and N. Engheta, Performing mathematical operations with metamaterials, Science **343**, 160 (2014).
[6] G. Ma and P. Sheng, Acoustic metamaterials: From local resonances to broad horizons, Sci. Adv. **2**, e1501595 (2016).
[7] B. Assouar, B. Liang, Y. Wu, Y. Li, J.-C. Cheng, and Y. Jing, Acoustic metasurfaces, Nat. Rev. Mater. **3**, 460 (2018).

[8] P.-Y. Chen, M. Farhat, S. Guenneau, S. Enoch, and A. Alù, Acoustic scattering cancellation via ultrathin pseudo-surface, Appl. Phys. Lett. **99**, 191913 (2011).

[9] G. Dupont, M. Farhat, A. Diatta, S. Guenneau, and S. Enoch, Numerical analysis of three-dimensional acoustic cloaks and carpets, Wave Motion **48**, 483 (2011).

[10] J. Mei, Z. Liu, J. Shi, and D. Tian, Theory for elastic wave scattering by a two-dimensional periodical array of cylinders: An ideal approach for band-structure calculations, Phys. Rev. B **67**, 245107 (2003).

[11] M. Farhat, P.-Y. Chen, H. Bağcı, S. Enoch, S. Guenneau, and A. Alu, Platonic scattering cancellation for bending waves in a thin plate, Sci. Rep. **4**, 1 (2014).

[12] M. Lapine, D. Powell, M. Gorkunov, I. Shadrivov, R. Marqués, and Y. Kivshar, Structural tunability in metamaterials, Appl. Phys. Lett. **95**, 084105 (2009).

[13] J. Qu, M. Kadic, A. Naber, and M. Wegener, Micro-structured two-component 3D metamaterials with negative thermal-expansion coefficient from positive constituents, Sci. Rep. **7**, 40643 (2017).

[14] P. M. Morse, Ku Ingard, theoretical acoustics, Princeton University Press, 949p **4**, 150 (1968).

[15] F. Zangeneh-Nejad and R. Fleury, Acoustic analogues of high-index optical waveguide devices, Sci. Rep. **8**, 1 (2018).

[16] S. Slussarenko, A. Alberucci, C. P. Jisha, B. Piccirillo, E. Santamato, G. Assanto, and L. Marrucci, Guiding light via geometric phases, Nat. Photonics **10**, 571 (2016).

[17] Y. Long, D. Zhang, C. Yang, J. Ge, H. Chen, and J. Ren, Realization of acoustic spin transport in metasurface waveguides, Nat. Commun. **11**, 1 (2020).

[18] M. Xiao, G. Ma, Z. Yang, P. Sheng, Z. Zhang, and C. T. Chan, Geometric phase and band inversion in periodic acoustic systems, Nat. Phys. **11**, 240 (2015).

[19] S. Wang, G. Ma, and C. T. Chan, Topological transport of sound mediated by spin-redirection geometric phase, Sci. Adv. **4**, eaaq1475 (2018).

[20] S. Wang, G. Zhang, X. Wang, Q. Tong, J. Li, and G. Ma, Spin-orbit interactions of transverse sound, Nat. Commun. **12**, 1 (2021).

[21] C. Caloz and Z.-L. Deck-Léger, Spacetime metamaterials–Part I: General concepts, IEEE Trans. Antennas Propag. **68**, 1569 (2019).

[22] C. Caloz and Z.-L. Deck-Léger, Spacetime metamaterials–Part II: Theory and applications, IEEE Trans. Antennas Propag. **68**, 1583 (2019).

[23] P. A. Huidobro, E. Galiffi, S. Guenneau, R. V. Craster, and J. Pendry, Fresnel drag in space–time-modulated metamaterials, Proc. Natl. Acad. Sci. **116**, 24943 (2019).

[24] E. Galiffi, P. Huidobro, and J. Pendry, Broadband Nonreciprocal Amplification in Luminal Metamaterials, Phys. Rev. Lett. **123**, 206101 (2019).

[25] M. Farhat, S. Guenneau, P.-Y. Chen, and Y. Wu, Spacetime modulation in floating thin elastic plates, Phys. Rev. B **104**, 014308 (2021).

[26] D. Censor and J. Aboudi, Scattering of sound waves by rotating cylinders and spheres, J. Sound Vib. **19**, 437 (1971).

[27] D. Censor and M. Schoenberg, Two dimensional wave problems in rotating elastic media, Appl. Sci. Res. **27**, 401 (1973).

[28] E. Graham and B. Graham, Effect of a shear layer on plane waves of sound in a fluid, J. Acoust. Soc. Am. **46**, 169 (1969).

[29] M. Schoenberg and D. Censor, Elastic waves in rotating media, Q. Appl. Math. **31**, 115 (1973).

[30] D. Ramaccia, D. L. Sounas, A. Alù, A. Toscano, and F. Bilotti, Doppler cloak restores invisibility to objects in relativistic motion, Phys. Rev. B **95**, 075113 (2017).

[31] S. Farhadi, Acoustic radiation of rotating and non-rotating finite length cylinders, J. Sound Vib. **428**, 59 (2018).

[32] D. Zhao, Y.-T. Wang, K.-H. Fung, Z.-Q. Zhang, and C. T. Chan, Acoustic metamaterials with spinning components, Phys. Rev. B **101**, 054107 (2020).

[33] M. Farhat, S. Guenneau, A. Alù, and Y. Wu, Scattering cancellation technique for acoustic spinning objects, Phys. Rev. B **101**, 174111 (2020).

[34] M. Farhat, P.-Y. Chen, M. Amin, A. Alù, and Y. Wu, Transverse acoustic spin and torque from pure spinning of objects, Phys. Rev. B **104**, L060104 (2021).

[35] R. Fleury, D. L. Sounas, C. F. Sieck, M. R. Haberman, and A. Alù, Sound isolation and giant linear nonreciprocity in a compact acoustic circulator, Science **343**, 516 (2014).

[36] L. Quan, S. Yves, Y. Peng, H. Esfahlani, and A. Alù, Odd Willis coupling induced by broken time-reversal symmetry, Nat. Commun. **12**, 1 (2021).

[37] Z. Yang, F. Gao, X. Shi, X. Lin, Z. Gao, Y. Chong, and B. Zhang, Topological Acoustics, Phys. Rev. Lett. **114**, 114301 (2015).

[38] Q. Wang, Z. Zhou, D. Liu, H. Ding, M. Gu, and Y. Li, Acoustic topological beam nonreciprocity via the rotational Doppler effect, Sci. Adv. **8**, eabq4451 (2022).

[39] W. Wang, C. Hu, J. Ni, Y. Ding, J. Weng, B. Liang, C.-W. Qiu, and J.-C. Cheng, Efficient and high-purity sound frequency conversion with a passive linear metasurface, Adv. Sci. **9**, 2203482 (2022).

[40] COMSOL Multiphysics, V5.6 (build: 280).

[41] See Supplemental Material at http://link.aps.org/supplemental/10.1103/PhysRevApplied.19.L041002 for a complete derivation of the governing equations and some numerical simulations of the waveguides.

[42] E. Dong, Z. Song, Y. Zhang, S. Ghaffari Mosanenzadeh, Q. He, X. Zhao, and N. X. Fang, Bioinspired metagel with broadband tunable impedance matching, Sci. Adv. **6**, eabb3641 (2020).

[43] S. Varghese, K. Gatos, A. Apostolov, and J. Karger-Kocsis, Morphology and mechanical properties of layered silicate reinforced natural and polyurethane rubber blends produced by latex compounding, J. Appl. Polym. Sci. **92**, 543 (2004).

[44] Z. Zou, R. Lirette, and L. Zhang, Orbital Angular Momentum Reversal and Asymmetry in Acoustic Vortex Beam Reflection, Phys. Rev. Lett. **125**, 074301 (2020).

[45] J. D. Jackson, *Classical Electrodynamics* (American Association of Physics Teachers, New York, 1999).

[46] D. Kupriyanov, I. Sokolov, and M. Havey, Antilocalization in coherent backscattering of light in a multi-resonance atomic system, Opt. Commun. **243**, 165 (2004).

[47] T. L. Singal, *Optical Fiber Communications: Principles and Applications* (Cambridge University Press, Cambridge, 2016).